Electronic Supplementary Material (ESI) for Journal of Materials Chemistry A.

Supplementary information

Unveiling the role of water in enhancing the performance of zinc-ion batteries using dimethyl sulfoxide electrolyte and the manganese dioxide cathode

Wathanyu Kao-ian[a], Jinnawat Sangsawang[a], Pinit Kidkhunthod[b], Suttipong Wannapaiboon[b], Manaswee Suttipong[c], Prasit Pattananuwat[d,e], Mai Thanh Nguyen[f], Tetsu Yonezawa[f] and Soorathep Kheawhom[a,e,g]

[a] Department of Chemical Engineering, Faculty of Engineering, Chulalongkorn University, Bangkok 10330, Thailand

[b] Synchrotron Light Research Institute, 111 University Avenue, Muang District, Nakhon Ratchasima 30000, Thailand

[c] Department of Chemical Technology, Faculty of Science, Chulalongkorn University, Bangkok 10330, Thailand

[d] Department of Materials Science, Faculty of Science, Chulalongkorn University, Bangkok 10330, Thailand

[e] Center of Excellence on Advanced Materials for Energy Storage, Chulalongkorn University, Bangkok 10330, Thailand

[f] Division of Materials Science and Engineering, Faculty of Engineering, Hokkaido University, Hokkaido 060-8628, Japan

[g] Bio-Circular-Green-economy Technology & Engineering Center (BCGeTEC), Faculty of Engineering, Chulalongkorn University, Bangkok 10330, Thailand

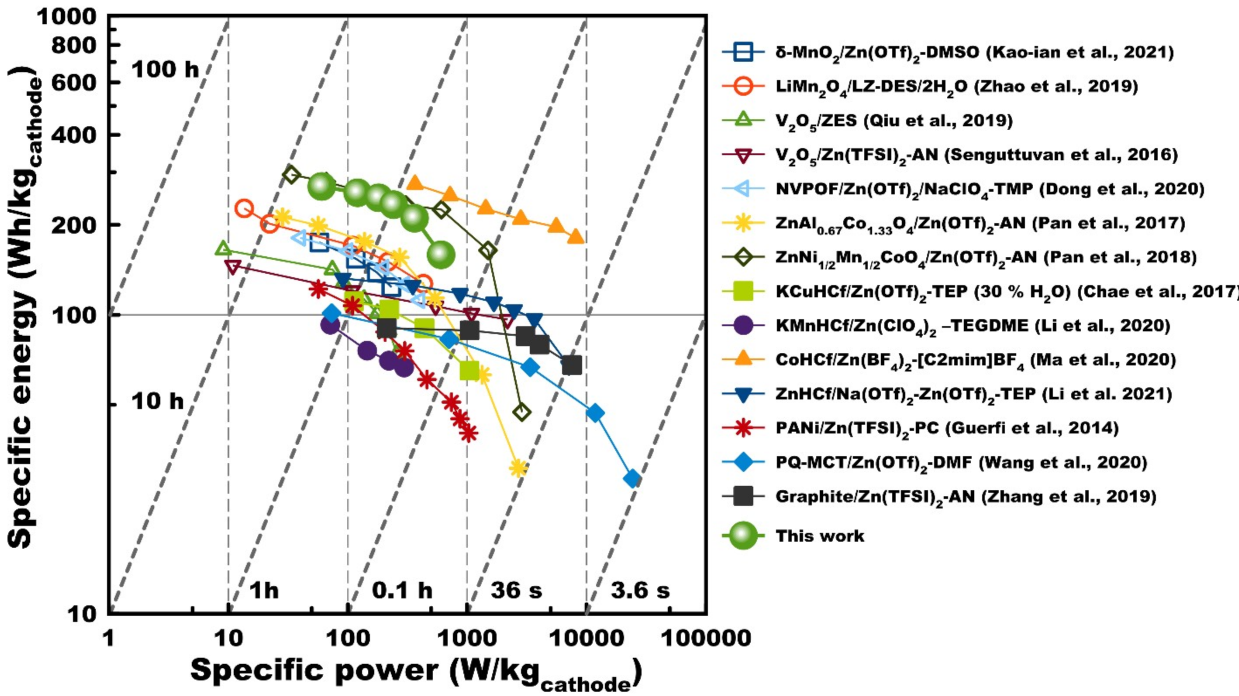

Figure S1. The Ragone plot of different nonaqueous zinc-ion batteries [1-15].

Table S1. Specific capacity of AZIBs based on MnO_2 cathodes.

Electrolyte	Phase of MnO_2	Testing window (V)	Specific capacity (mAh/g)	Ref.
Aqueous 1 M $ZnSO_4$	α-MnO_2	1.0-1.8 V	233 mAh/g at 83 mA/g	[16]
Aqueous 2 M $ZnSO_4$ + 0.1 M $MnSO_4$	α-MnO_2	1.0-1.8 V	285 mAh/g at 103 mA/g	[17]
Aqueous 1 M $ZnSO_4$ + 0.1 M $MnSO_4$	β-MnO_2	1.0-1.8 V	270 mAh/g at 100 mA/g	[18]
Aqueous 3 M $Zn(CF_3SO_3)_2$ + 0.1 M $Mn(CF_3SO_3)_2$	β-MnO_2	0.8-1.9 V	225 mAh/g at 0.65 C	[19]
Aqueous 1 M $ZnSO_4$	δ-MnO_2	1.0-1.8 V	252 mAh/g at 83 mA/g	[20]
Aqueous 1 M $ZnSO_4$ + 0.1 M $MnSO_4$	δ-MnO_2	1.0-1.8 V	170 mAh/g at 100 mA/g	[21]

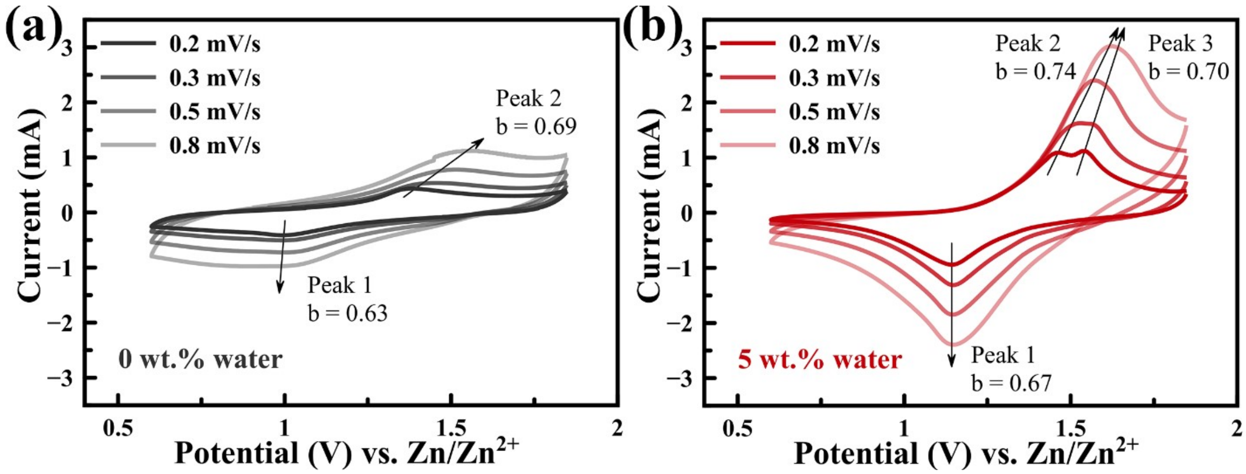

Figure S2. CV curves of sample having (a) 0 wt.% water, and (b) 5 wt.% water at 0.2, 0.3, 0.5 and 0.8 mV/s in the range: 0.6-1.85 V vs. Zn/Zn^{2+}.

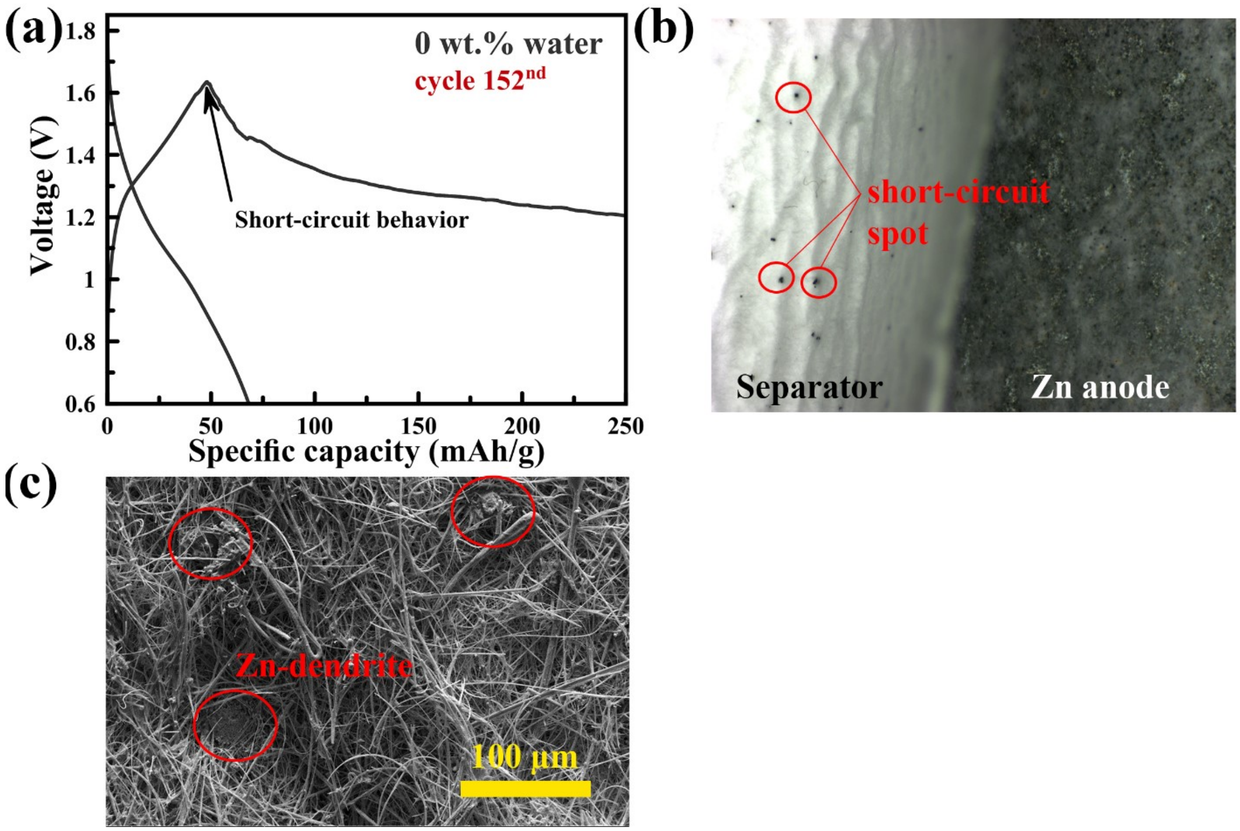

Figure S3. Evidence of the short-circuit occurred in the 0 wt.% water sample: (a) Voltage profile at 152rd cycles, (b) Image obtained via optical microscope of the anode/separator contact, and (c) FE-SEM image of the dark spot on the separator.

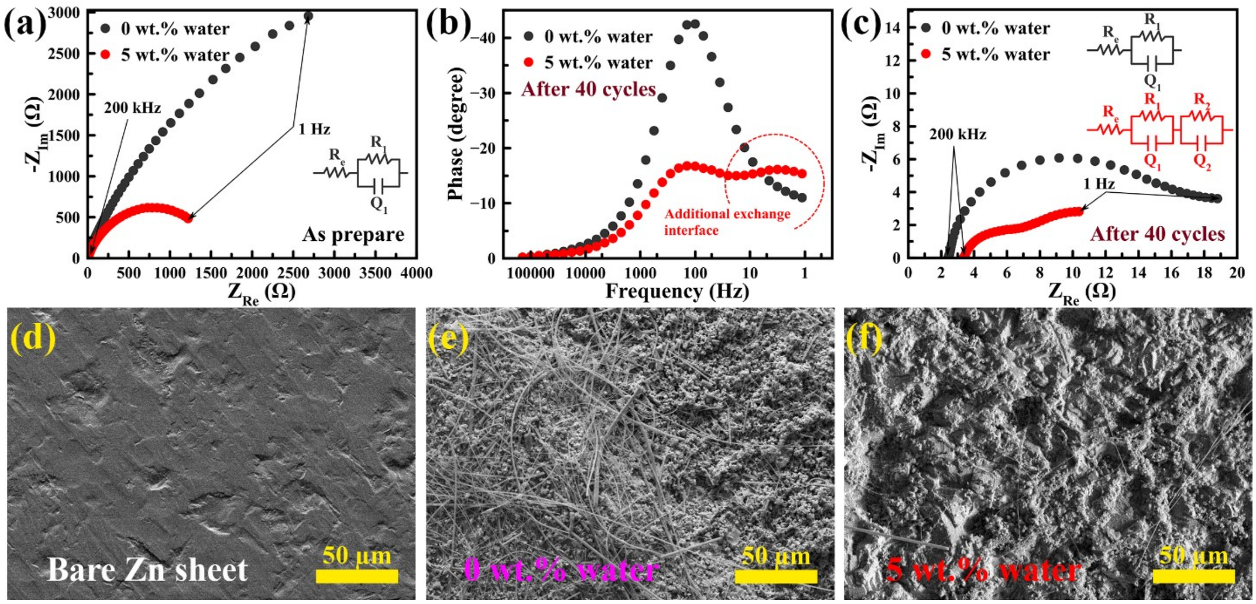

Figure S4. (a-c) EIS results of the Zn symmetrical cells: (a) Nyquist plot of the as-prepare sample, (b) Phase-bode plot of the cycled samples (40th cycle), and (c) Nyquist plot of the cycled samples (40th cycle), (d-e) FE-SEM images: (d) Bare Zn sheet, (e) 0 wt.% water sample, and (f) 5 wt.% water sample.

Table S2. EIS fitting results of Zn symmetrical cells: 0 and 5 wt.% water.

Components	**0 wt.% water (As prepare)**	**0 wt.% water (After 40th)**	**5 wt.% water (As prepare)**	**5 wt.% water (After 40th)**
Internal resistance of the cell: $\mathbf{R_e}$	**2.23 Ω**	**2.43 Ω**	**3.38 Ω**	**3.37 Ω**
Charge-transfer resistance of the Zn electrode: $\mathbf{R_1}$	**8.91×10^3 Ω**	**14.58 Ω**	**1.63×10^3 Ω**	**3.65 Ω**
Capacitive double layer of the Zn electrode: $\mathbf{Q_1}$ **($\mathbf{Y_0}$, n)**	**3.91×10^{-5}, 0.8**	5.39×**10^{-4}, 0.89**	**6.712×10^{-5}, 0.82**	**1.99×10^{-3}, 0.77**
Charge-transfer resistance of the additional exchange interface: $\mathbf{R_2}$	**-**	**-**	**-**	**7.30 Ω**
Capacitive double layer of the additional exchange interface: $\mathbf{Q_2}$ **($\mathbf{Y_0}$, n)**	**-**	**-**	**-**	2.20×**10^{-2}, 0.79**

Table S3. EIS fitting results of the full cells: 0 and 5 wt.% water.

Components	**0 wt.% water (After 10th)**	**5 wt.% water (After 10th)**
Internal resistance of the battery: $\mathbf{R_e}$	2.28 Ω	2.93 Ω
Charge-transfer resistance of the Zn anode: $\mathbf{R_1}$	4.09 Ω	1.52 Ω
Capacitive double layer of the Zn anode: $\mathbf{C_1}$	1.07×10^{-5} F	1.16E$\times10^{-5}$ F
Charge-transfer resistance of the MnO_2 cathode: $\mathbf{R_2}$	15.27 Ω	8.85 Ω
Capacitive double layer of the MnO_2 cathode: $\mathbf{Q_2}$ **($\mathbf{Y_0}$, n)**	4.85×10^{-3}, 0.75	3.59×10^{-3}, 0.75
Warburg diffusion impedance of the MnO_2 cathode: **W ($\mathbf{Y_0}$)**	1.86×10^{-2}	7.15×10^{-2}

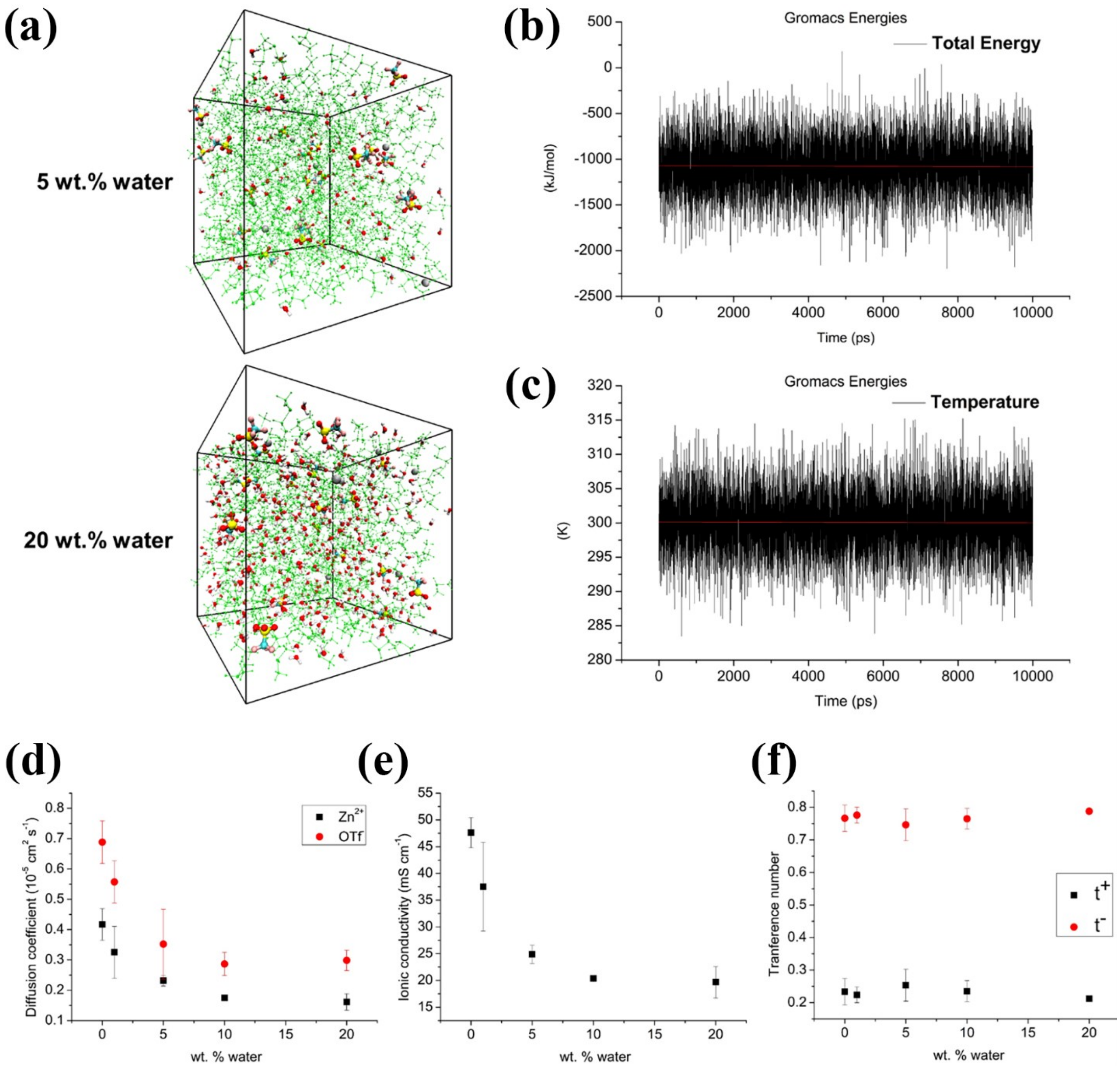

Figure S5. MD simulation results of bulk electrolyte solutions, consisting of $Zn(OTf)_2$ in DMSO with the addition of water: (a) Examples of simulation boxes, including 5 wt.% water and 20 wt.% water added electrolytes, (b) Total energy analysis of 5 wt.% water added system, (c) Equilibrated temperature plot of 5 wt.% water added system, (d) Diffusion coefficient of Zn^{2+} and OTf^-, (e) Ionic conductivity of electrolytes, and (f) Transference number.

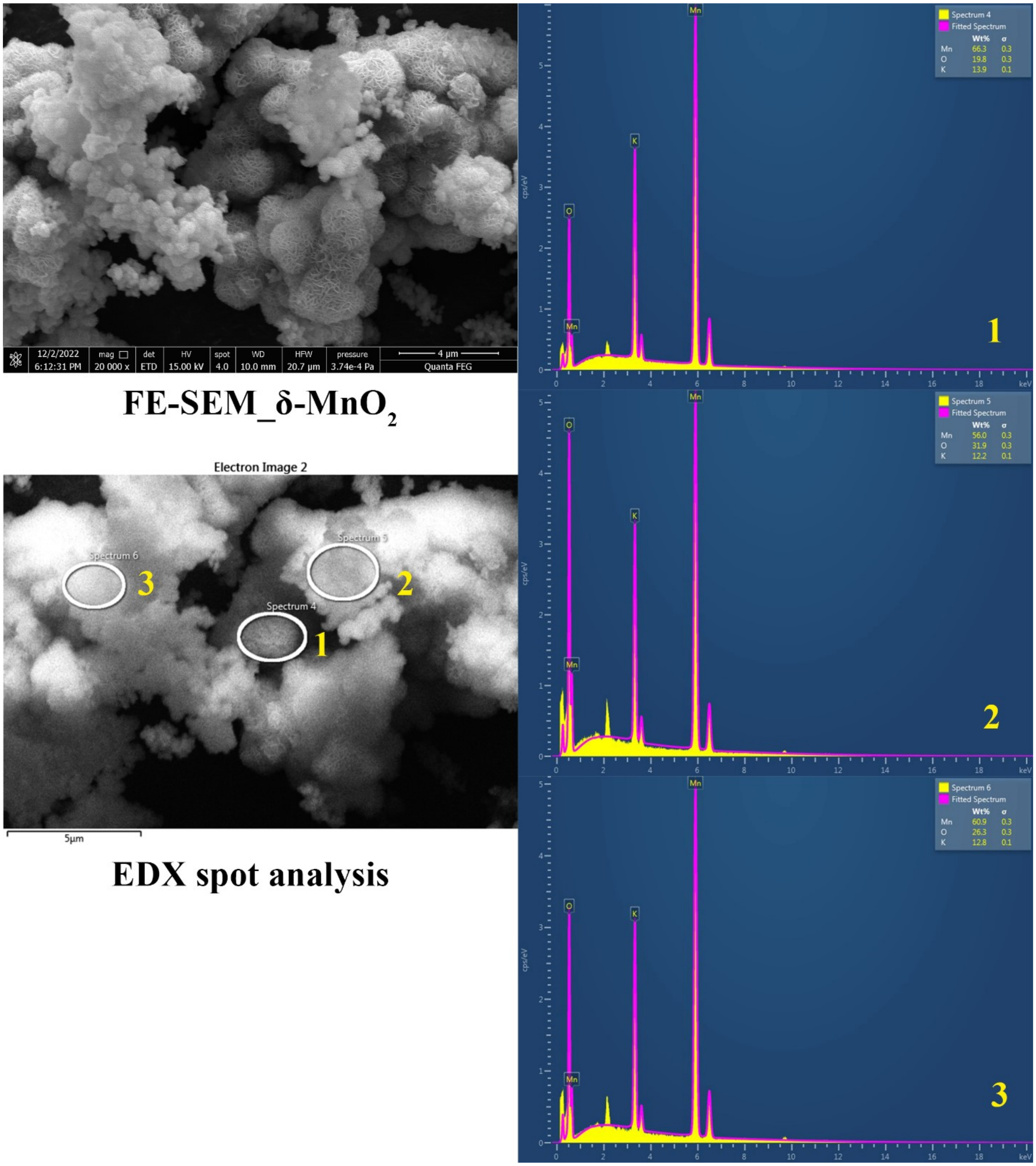

Figure S6. EDX-Spectra of the synthesized MnO_2 recorded by spot analysis.

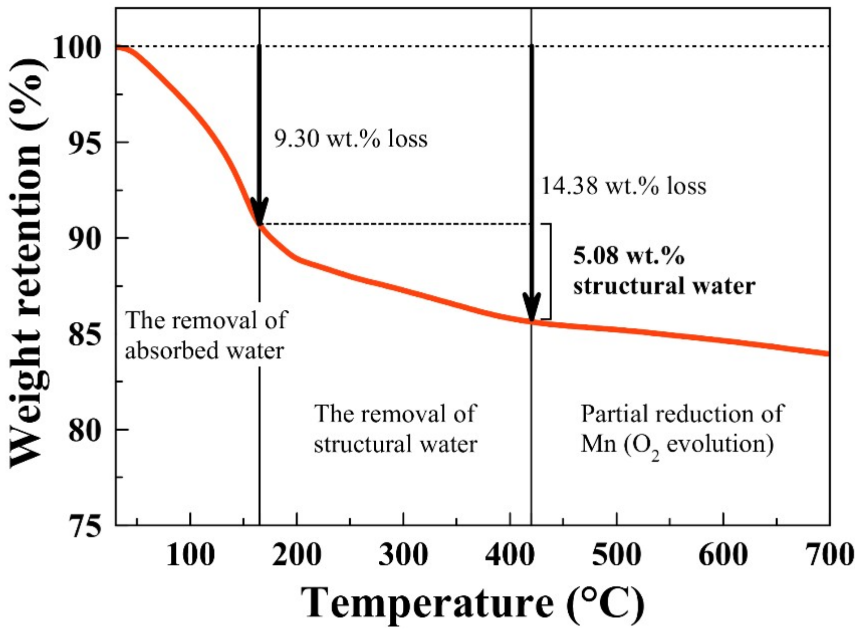

Figure S7. TGA result of the synthesized MnO_2: scan rate of 5 °C per min at T = 30-700 °C.

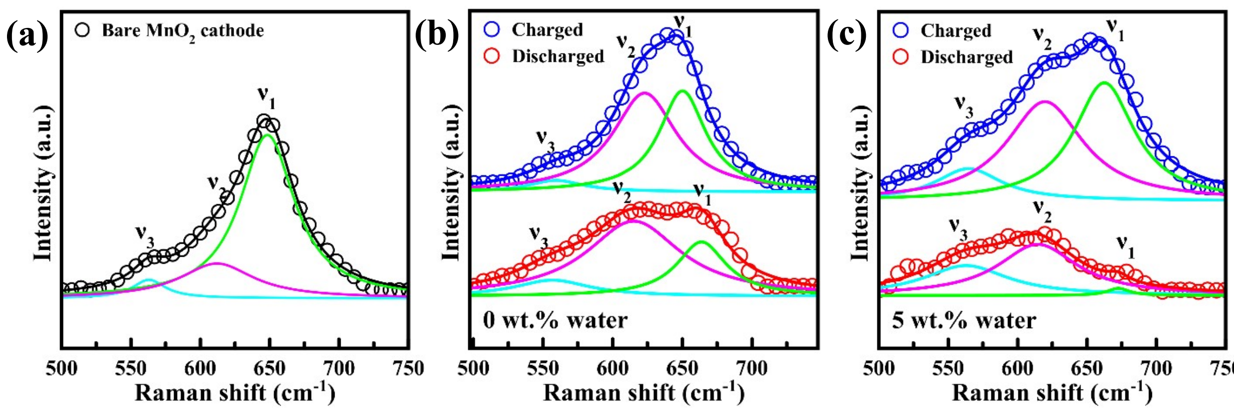

Fig. S8. Lorentzian fitting results of the Raman spectra of: (a) Bare δ-MnO_2 cathode, (b) 0 wt.% sample, and (c) 5 wt.% sample.

Raman bands: ν_1, ν_2 and ν_3, which can be assigned to a symmetric stretching vibration of Mn-O band in the MnO_6 octahedra, a Mn-O lattice vibration and a Mn-O lattice vibration of the basal plane of the MnO_2 sheets, respectively, existed in both charged and discharged cathode of both 0 and 5 wt.% samples, indicating that a "layered to layered" transformation occurred in both the 0 and 5 wt.% sample [22]. Upon the discharging, ν_1 of both the 0 and 5 wt.% proceeded to the higher wave number (blue shift), whereas ν_2 shifted to the lower wave number (red shift), indicating the decrease of Mn oxidation number and the elongation of MnO_6 unit cell (Jahn–Teller distortion) [23].

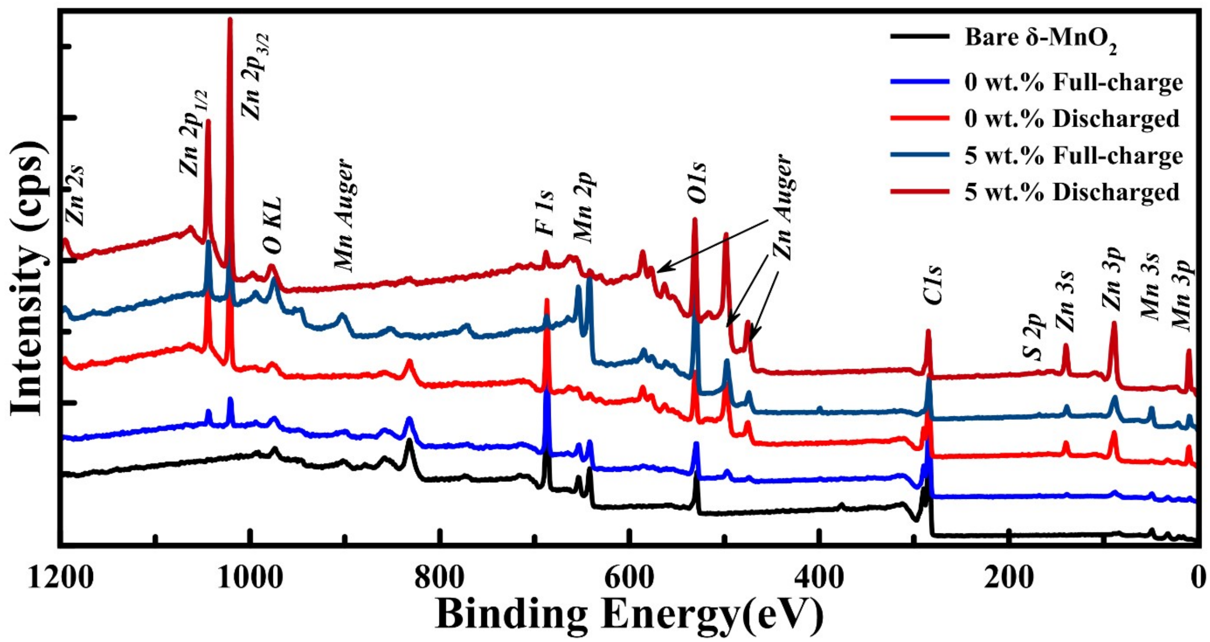

Figure S9. Wide scan XPS of all cathodes: binding energy range of 0-1200 eV.

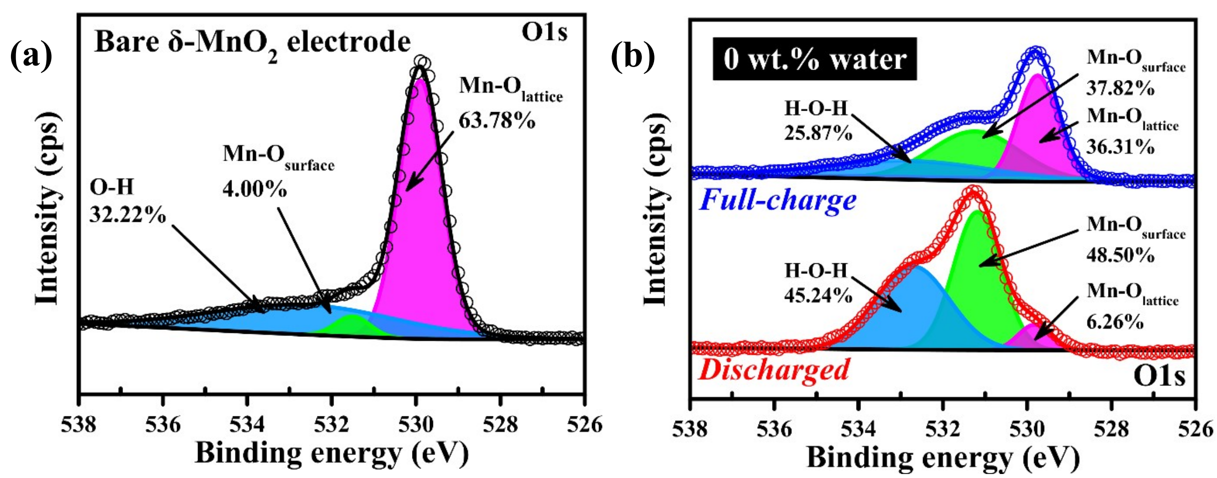

Figure S10. O1s XPS spectrum of: (a) the bare δ-MnO_2 cathode and (b) the 0 wt.% water sample.

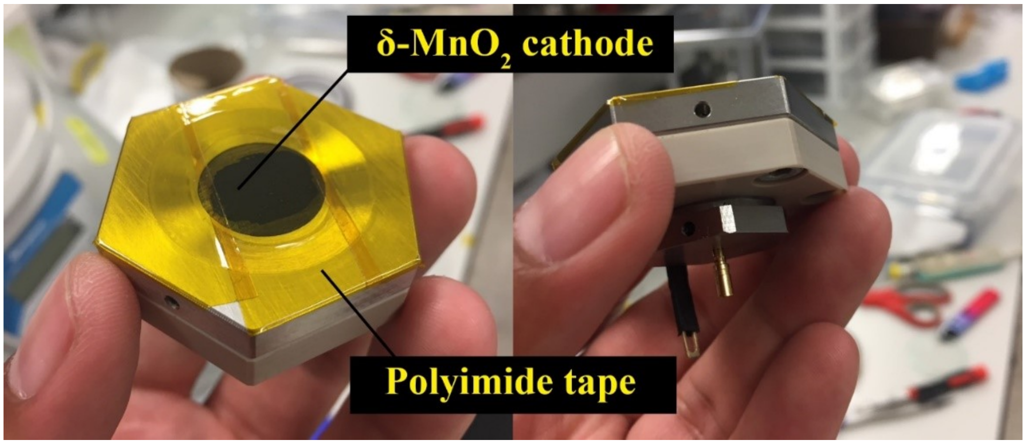

Figure S11. Swagelok type cell for the operando XRD.

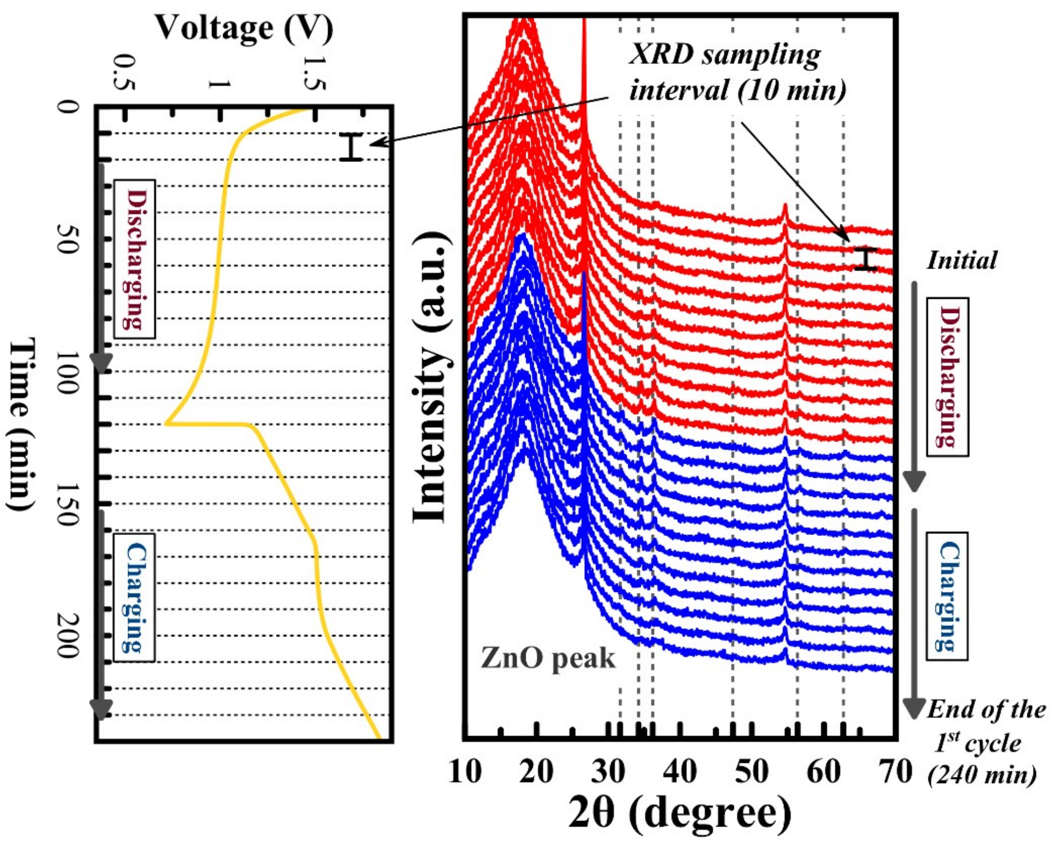

Figure S12. Operando XRD spectra of the Zn/MnO_2 battery having 5 wt.% water DMSO within angle (2theta) of 10-70°.

References

1. W. Kao-ian, M. T. Nguyen, T. Yonezawa, R. Pornprasertsuk, J. Qin, S. Siwamogsatham and S. Kheawhom, Materials Today Energy, 2021, DOI: 10.1016/j.mtener.2021.100738, 100738, DOI: 10.1016/j.mtener.2021.100738.

2. J. Zhao, J. Zhang, W. Yang, B. Chen, Z. Zhao, H. Qiu, S. Dong, X. Zhou, G. Cui and L. Chen, Nano Energy, 2019, 57, 625-634, DOI: 10.1016/j.nanoen.2018.12.086.

3. H. Qiu, X. Du, J. Zhao, Y. Wang, J. Ju, Z. Chen, Z. Hu, D. Yan, X. Zhou and G. Cui, Nature Communications, 2019, 10, 5374, DOI: 10.1038/s41467-019-13436-3.

4. P. Senguttuvan, S.-D. Han, S. Kim, A. L. Lipson, S. Tepavcevic, T. T. Fister, I. D. Bloom, A. K. Burrell and C. S. Johnson, Advanced Energy Materials, 2016, 6, 1600826, DOI: 10.1002/aenm.201600826.

5. Y. Dong, S. Di, F. Zhang, X. Bian, Y. Wang, J. Xu, L. Wang, F. Cheng and N. Zhang, Journal of Materials Chemistry A, 2020, 8, 3252-3261, DOI: 10.1039/C9TA13068C.

6. C. Pan, R. G. Nuzzo and A. A. Gewirth, Chem. Mater., 2017, 29, 9351-9359, DOI: 10.1021/acs.chemmater.7b03340.

7. C. Pan, R. Zhang, R. G. Nuzzo and A. A. Gewirth, Advanced Energy Materials, 2018, 8, 1800589, DOI: 10.1002/aenm.201800589.

8. M. S. Chae, J. W. Heo, H. H. Kwak, H. Lee and S.-T. Hong, J. Power Sources, 2017, 337, 204-211, DOI: 10.1016/j.jpowsour.2016.10.083.

9. Q. Li, K. Ma, G. Yang and C. Wang, Energy Storage Materials, 2020, 29, 246-253, DOI: 10.1016/j.ensm.2020.04.030.

10. L. Ma, S. Chen, N. Li, Z. Liu, Z. Tang, J. A. Zapien, S. Chen, J. Fan and C. Zhi, Adv. Mater., 2020, 32, 1908121, DOI: 10.1002/adma.201908121.

11. A. Guerfi, J. Trottier, I. Boyano, I. De Meatza, J. A. Blazquez, S. Brewer, K. S. Ryder, A. Vijh and K. Zaghib, J. Power Sources, 2014, 248, 1099-1104, DOI: 10.1016/j.jpowsour.2013.09.082.

12. N. Wang, X. Dong, B. Wang, Z. Guo, Z. Wang, R. Wang, X. Qiu and Y. Wang, Angew. Chem. Int. Ed., 2020, 59, 14577-14583, DOI: 10.1002/anie.202005603.

13. N. Zhang, Y. Dong, Y. Wang, Y. Wang, J. Li, J. Xu, Y. Liu, L. Jiao and F. Cheng, ACS Applied Materials & Interfaces, 2019, 11, 32978-32986, DOI: 10.1021/acsami.9b10399.

14. L. Miao, R. Wang, W. Xin, L. Zhang, Y. Geng, H. Peng, Z. Yan, D. Jiang, Z. Qian and Z. Zhu, Energy Storage Materials, 2022, 49, 445-453, DOI: 10.1016/j.ensm.2022.04.032.

15. W. Kao-ian, A. A. Mohamad, W.-R. Liu, R. Pornprasertsuk, S. Siwamogsatham and S. Kheawhom, Batteries & Supercaps, 2022, 5, e202100361, DOI: 10.1002/batt.202100361.

16. M. H. Alfaruqi, J. Gim, S. Kim, J. Song, J. Jo, S. Kim, V. Mathew and J. Kim, Journal of Power Sources, 2015, 288, 320-327, DOI: 10.1016/j.jpowsour.2015.04.140.

17. H. Pan, Y. Shao, P. Yan, Y. Cheng, K. S. Han, Z. Nie, C. Wang, J. Yang, X. Li, P. Bhattacharya, K. T. Mueller and J. Liu, Nature Energy, 2016, 1, 16039, DOI: 10.1038/nenergy.2016.39.

18. S. Islam, M. H. Alfaruqi, V. Mathew, J. Song, S. Kim, S. Kim, J. Jo, J. P. Baboo, D. T. Pham, D. Y. Putro, Y.-K. Sun and J. Kim, Journal of Materials Chemistry A, 2017, 5, 23299-23309, DOI: 10.1039/C7TA07170A.

19. N. Zhang, F. Cheng, J. Liu, L. Wang, X. Long, X. Liu, F. Li and J. Chen, Nature Communications, 2017, 8, 405, DOI: 10.1038/s41467-017-00467-x.

20. M. H. Alfaruqi, J. Gim, S. Kim, J. Song, D. T. Pham, J. Jo, Z. Xiu, V. Mathew and J. Kim, Electrochem. Commun., 2015, 60, 121-125, DOI: 10.1016/j.elecom.2015.08.019.

21. C. Guo, H. Liu, J. Li, Z. Hou, J. Liang, J. Zhou, Y. Zhu and Y. Qian, Electrochimica Acta, 2019, 304, 370-377, DOI: 10.1016/j.electacta.2019.03.008.

22. Y. Jiang, D. Ba, Y. Li and J. Liu, Advanced Science, 2020, 7, 1902795, DOI: 10.1002/advs.201902795.

23. L. Liu, L. Su, Y. Lu, Q. Zhang, L. Zhang, S. Lei, S. Shi, M. D. Levi and X. Yan, Advanced Functional Materials, 2019, 29, 1806778, DOI: 10.1002/adfm.201806778.